Tellus (1997), 49A, 613–621
Printed in UK – all rights reserved

TELLUS
ISSN 0280–6495

Seasonal variation of global surface pressure and water vapor

By TSING-CHANG CHEN*, JAU-MING CHEN, SIEGFRIED SCHUBERT and LAWRENCE L. TAKACS, *Atmospheric Science Program, Department of Geological and Atmospheric Sciences, Iowa State University, USA and Data Assimilation office, Laboratory for Atmospheres, Goddard Space Flight Center/NASA, USA*

(Manuscript received 11 March 1997; in final form 7 July 1997)

ABSTRACT

Previous studies have shown that the seasonal variation of global-mean surface pressure (p_s) results from variation of global-mean water vapor pressure (p_w). The current study, employing the global data generated by Version 1 of the Goddard Earth Observing System (GEOS-1) Data Assimilation System, shows that seasonal variations of *regional* p_s and p_w tend to be out of phase (particularly in the subtropics of the two hemispheres) and that the magnitude of the former variation is generally much larger than that of the latter. The seasonal variations of these two quantities are maintained by airmass and water vapor transports by the global divergent circulation, which is driven by the latent heat released by cumulus convection over the water vapor sink, as the "water mass forcing" mechanism predicted. Since p_w and p_s are used often in depicting the climate system, assessments of climate change in terms of the global-mean and regional variations of these two variables should be interpreted with caution.

1. Introduction

The seasonal variation of atmospheric circulation is the most pronounced signal of climate variation. Since surface pressure (p_s) is often used in depicting the climate system, the understanding of physical processes maintaining the p_s seasonal variation would be of use to our search for the cause of climate variation. It follows from the conservation of dry airmass that the seasonal variation of global-mean p_s is originated by the seasonal variation of global-mean water vapor pressure (p_w) (e.g., Van den Dool and Saha 1993). These coherent seasonal variations of p_s and p_w may, however, not hold hemispherically and regionally. For example, hemispheric-mean p_s and p_w vary seasonally in an opposite phase (Trenberth et al. 1987). The maximum interhemispheric transport of airmass occurs in late boreal spring from the Northern to Southern Hemisphere and the reversed transport happens in early boreal fall (Trenberth et al. 1987). Water vapor is transported from the winter to the summer hemisphere (Chen et al. 1996). From a regional perspective, Boer (1986) introduced the potential function and divergent component of airmass flux; van den Dool and Saha (1993) demonstrated that the maximum mass flux occurs during the transition months from regions of positive to regions of negative pressure tendency. Using divergent water vapor flux vectors, Chen et al. (1995) showed that the seasonal variation of global precipitable water is maintained by three pairs of water vapor flux divergence-convergence centers located over the

* Corresponding author.
Corresponding author address: Tsing-Chang Chen, Atmospheric Science Program, Department of Geological and Atmospheric Sciences, 3010 Agronomy Hall, Iowa State University, Ames, IA 50011, USA.

three tropical continents; centers on each side of the equator are in the same sign.

The above and other studies dealing with seasonal variations of p_s and p_w, raise a number of questions. These include the following.

(1) What are the regional relationships between the seasonal variations of p_s and p_w over different areas of the globe (if any)?

(2) Van den Dool and Saha (1993) proposed the concept of *water mass forcing* which is *a mechanism for atmospheric circulation to be driven by water mass sinks and sources*. What is the link between the regional atmospheric circulation and water vapor transport within the seasonal variation context?

In order to answer these two questions, this study analyzes the airmass and water-vapor pressure budgets employing the reanalysis data generated by Version 1 of the Goddard Earth Observing System (GEOS-1)-Data Assimilation System (DAS) (Schubert et al. 1993) for a 9-year period (1985–1993). The GEOS-1-DAS products are arrayed at a horizontal resolution of 2° lat. × 2.5° long. and 20 sigma levels (or 18 pressure levels), and include 3-h precipitation and evaporation data generated by the GEOS-DAS model during the course of the assimilation. While the precipitation and evaporation estimates have a substantial bias (Schubert et al. 1995), seasonal variations of major elements of the global water vapor budget depicted by the GEOS-1 data (in Sections 2 and 3) are relatively coherent.

2. Budget analysis

2.1. Budget equations

By integrating the continuity equation over the entire depth of the atmosphere, one obtains the surface pressure tendency equation of dry airmass (e.g., van den Dool and Saha 1993):

$$\frac{\partial p_d}{\partial t} = -g\nabla\cdot M_d\,, \tag{1}$$

where M_d, p_d, and g are the vertically-integrated dry airmass flux, the surface pressures of dry airmass, and gravity, respectively. The water vapor pressure is $p_w = g\,W$, where

$$W = \frac{1}{g}\int_0^{p_s} q\,\mathrm{d}p$$

(precipitable water) and q is specific humidity. Based upon the water vapor budget equation, the p_w tendency may be written as

$$\frac{\partial p_w}{\partial t} = -g\nabla\cdot Q + g\,(E-P), \tag{2}$$

where Q, E, and P are the vertically-integrated water-vapor flux, evaporation and precipitation, respectively. Since $p_s = p_d + p_w$, one may combine eqs. (1) and (2) to form the total surface pressure tendency equation

$$\frac{\partial p_s}{\partial t} = -g\nabla\cdot M + g\,(E-P), \tag{3}$$

where $M = M_d + Q$. The regional surface pressure tendency is caused not only by the convergence of dry airmass flux, but also by the convergence of water vapor flux and the in-situ water vapor source/sink $(E-P)$.

For convenience of discussion, let us write out the global $[\ ]_{GB}$ and hemispheric $[\ ]_{()H}$ budget equations of p_d, p_s and p_w. The globally-integrated tendencies are:

$$\frac{\partial [p_d]_{GB}}{\partial t} = 0, \tag{4}$$

$$\frac{\partial [p_s]_{GB}}{\partial t} = \frac{\partial [p_w]_{GB}}{\partial t} = g[E-P]_{GB}\,. \tag{5}$$

As revealed from these two equations, $[p_d]$ is conserved and annual variations of $[p_s]_{GB}$ and $[p_w]_{GB}$ are coincident.

Climatologically, the Southern (SH) and Northern (NH) Hemispheres are water vapor source and sink hemispheres (Chen et al. 1996), respectively. Since $[\nabla\cdot M]_{GB} = 0$ and $[\nabla\cdot Q]_{GB} = 0$, one may expect $[\nabla\cdot M]_{NH} = -[\nabla\cdot M]_{SH}$ and $[\nabla\cdot Q]_{NH} = -\ [\nabla\cdot Q]_{SH}$. For these reasons, we thus use the SH divergences of dry airmass and water vapor fluxes to formulate the hemispheric budget equations:

$$\frac{\partial [p_d]_{NH}}{\partial t} = g[\nabla\cdot M_d]_{SH}\,, \tag{6}$$

$$\frac{\partial [p_d]_{SH}}{\partial t} = -\ g[\nabla\cdot M_d]_{SH}\,, \tag{7}$$

and,

$$\frac{\partial [p_w]_{NH}}{\partial t} = g[\nabla \cdot Q]_{SH} + g[E-P]_{NH}\,, \qquad (8)$$

$$\frac{\partial [p_w]_{SH}}{\partial t} = -\ g[\nabla \cdot Q]_{SH} + g[E-P]_{SH}\,. \qquad (9)$$

Note that

$$[\nabla \cdot M_d]_{SH} = \frac{2\,\pi a}{g}\langle v_z \rangle \text{ and} \qquad (10)$$
$$[\nabla \cdot Q]_{SH} = 2\pi a (Q_\phi)_z\,,$$

where

$$\langle\ \rangle \equiv \int_0^{p_s} (\ ) \mathrm{d}p \text{ and } (\ )_z = \frac{1}{2\pi}\int_0^{2\pi} (\ )\ \mathrm{d}\lambda,$$

and v and Q_ϕ are meridional components of wind and water vapor flux, respectively. The Hadley circulation is responsible for v_Z and $(Q_\phi)_Z$ across the equator.

2.2. Global budget

The major goal of this study is to examine the regional relationship between seasonal variations of p_s and p_w. However, before tackling this problem, it would be informative to find out to what extent seasonal variations of $[p_s]_{GB}$ and $[p_w]_{GB}$ portrayed by the GEOS-1 data satisfy the global constraints of eqs. (4) and (5). Both $[p_s]_{GB}$ and $[p_w]_{GB}$ vary seasonally in a coherent manner with an amplitude of about 0.4 mb (not shown). These two quantities reach their maximum and minimum in boreal summer and winter, respectively. Thus, one can expect a boreal spring buildup and boreal fall decline of both $[p_s]_{GB}$ and $[p_w]_{GB}$ (as shown in Fig. 1). Although seasonal variations of $\partial[p_s]_{GB}/\partial t$ and $\partial[p_w]_{GB}/\partial t$ are by and large synchronous, the amplitude discrepancy between them indicates that $[p_d]_{GB}$ contained in the GEOS-1 data may not exactly conserved.

Since $[E-P]_{GB}$ is the source/sink of water vapor, seasonal variations of both $\partial[p_w]_{GB}/\partial t$ and $g[E-P]_{GB}$ should coincide. Even though the GEOS Data Assimilation System employs increment analysis update procedure to reduce initial imbalances and spinup (Bloom et al. 1991), there is no constraint that forces the initial fields of p_w and $(E-P)$ to satisfy eq. (5). It is shown in Fig. 1 that the overall seasonal variation of $g[E-P]_{GB}$ follows closely that of $\partial[p_w]_{GB}/\partial t$, except that the amplitude of the latter is smaller than the former. Integrating eq. (5) to obtain $[p_w]_{GB}$ with $[E-P]_{GB}$ generated directly by the NCEP(National Center for Environmental Prediction)/NCAR (National Center for Atmopshric Research) reanalysis, Van den Dool et al. (1995) found the following: the seasonal variation of integrated $[p_w]_{GB}$ is close to real $[p_s]_{GB}$ when $[E-P]_{GB}<0$ in the second half of the year. As revealed from Fig. 1, amplitudes of $\partial[p_s]_{GB}/\partial t$ and $g[E-P]_{GB}$ are more comparable, but larger than the amplitude of $\partial[p_w]_{GB}/\partial t$, particularly in the second half of the year. Based upon van den Dool et al.'s finding, the integrated $[p_w]_{GB}$, and in turn $[p_s]_{GB}$, with the GEOS-1 data should decline faster than real $[p_w]_{GB}$. The comparison between seasonal variations of $[p_s]_{GB}$ and $[p_w]_{GB}$ of the GEOS-1 data (not shown) confirms this argument.

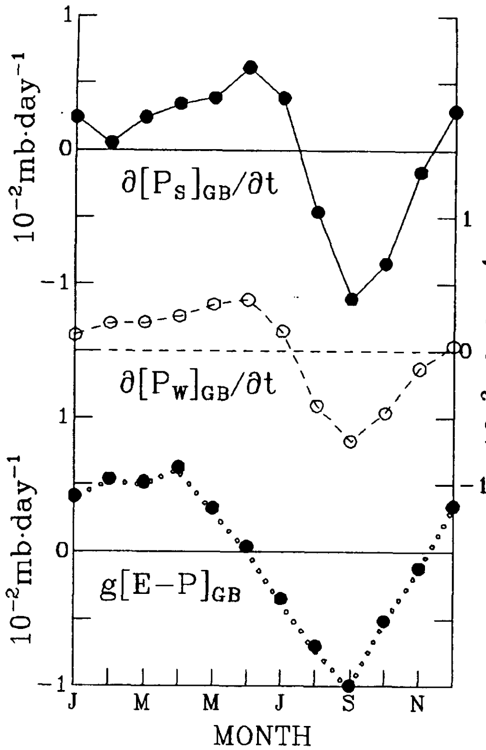

Fig. 1. Annual variation of global-mean monthly surface pressure tendency $\partial[p_s]GB/\partial t$, and of water vapor pressure tendency $\partial[p_{w]GB}/\partial t$ and $g[E-P]_{GB}$ averaged over 1985–1993.

2.3. Hemispheric budget

As shown in eqs. (6)-(7) and (10), the hemispheric-mean p_d tendency is balanced by the inter-hemispheric airmass exchange across the equator, which is accomplished by the Hadley circulation. Fig. 2a shows the hemispheric-mean p_d budget; the minimum and maximum hemispheric-mean p_d tendencies of the two hemispheres occur in spring and fall, respectively, for each hemisphere. In order to maintain the hemispheric-mean p_d tendencies, airmass must be transported from one hemisphere to compensate the airmass change of the other hemisphere. Conceivably, the former hemispheric-mean $\nabla \cdot M_d$ should reach its maximum (minimum) in spring (fall). The seasonal variation of $g[\nabla \cdot M_d]_{SH}$ $(= -g[\nabla \cdot M_d]_{NH}$ shown in Fig. 2a coincides well with those of the hemispheric-mean p_d tendencies in the two hemispheres. This agreement indicates that seasonal variations of the hemispheric-mean p_d budgets are properly depicted by the GEOS-1 data.

Shown in Fig. 2b are the hemispheric-mean p_w budgets of the two hemispheres with the following salient features.

(1) The hemispheric-mean $g(E-P)$ reaches its

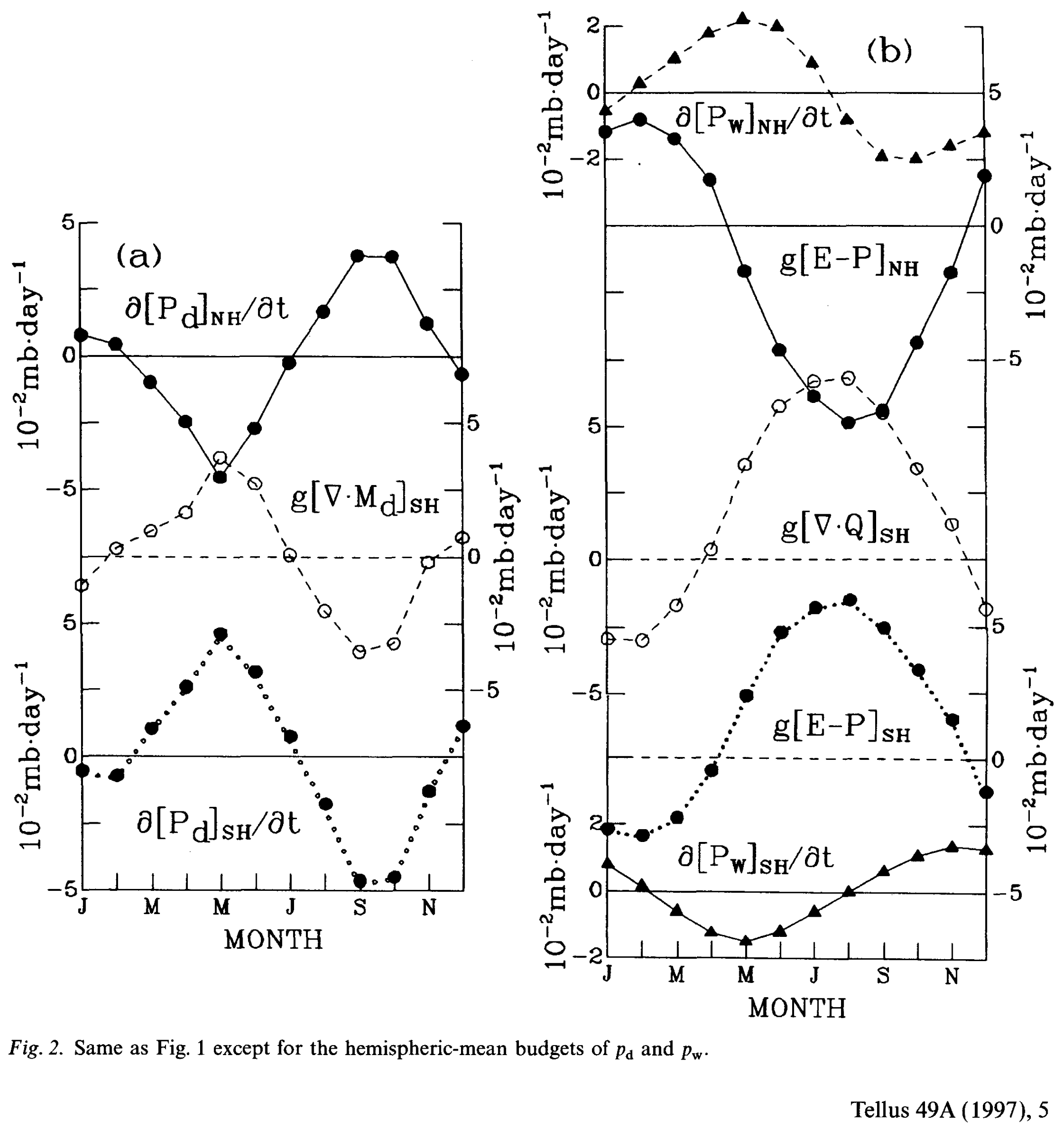

Fig. 2. Same as Fig. 1 except for the hemispheric-mean budgets of p_d and p_w.

maximum (minimum) in winter (summer). $(E-P)$ is the water vapor source/sink. To balance the seasonal variation of $(E-P)$ in both hemispheres, water vapor should be transported across the equator from the winter to the summer hemisphere by the Hadley circulation. Water vapor exists mainly in the lower troposphere so that the equator-crossing water vapor transport is carried out by the lower branch of the Hadley circulation. The seasonal variation of $[\nabla \cdot Q]_{SH}$, for example, follows that of $[E-P]_{SH}$.

(2) The Hadley circulation is responsible for both $[\nabla \cdot Q]_{SH}$ and $[\nabla \cdot M_d]_{SH}$, but a quadrature phase lag exists between seasonal variations of these two physical processes. Because of this temporal phase difference, one may wonder whether there is a coherent seasonal variation of hemispheric-mean p_d and p_w. According to eqs. (8) and (9), the hemispheric-mean p_w tendency is determined by the summation of hemispheric-mean $g\nabla \cdot Q$ and $g(E-P)$. It is revealed from the contrast between Figs. 2a and 2b that seasonal variations of hemispheric-mean p_d and p_w tendencies are *opposite* in phase. In other words, the spring (fall) buildup (decline) of hemispheric-mean p_w is in accordance with the spring (fall) decline (buildup) of hemispheric-mean p_d. This out-of-phase relationship between the hemispheric-mean p_d and p_w tendencies results from the fact that the spring (fall) export (import) of water vapor by the Hadley circulation is larger (smaller) than the spring (fall) hemispheric-mean $(E-P)$.

In view of the contrast between seasonal variations of the hemispheric-mean p_d and p_w budgets, we realize that the water vapor transport is not the only hydrological process responsible for the seasonal variation of the hemispheric-mean p_w; we also need to take the water vapor source/sink into account.

The discussion of the relationship between seasonal variations of p_s and p_w is thus far based upon the global/hemispheric-mean airmass and water-vapor budget. In other words, we illustrate only the possible roles of surface pressure and the hydrological cycle in the climate system in a global/hemispheric mean sense. In fact, there exist pronounced asymmetric components of both p_s and p_w (or W) in their global distributions. These asymmetric components of p_s and p_w are integral parts of the global climate system. To understand the relationship between seasonal variations of local p_s and p_w, the local maintenance of the p_s and p_w should be examined. An effort along this line is made in the next section.

3. Global distribution of surface pressure and water-vapor budget

From a global perspective, the seasonal variations of $[p_s]_{GB}$ and $[p_w]_{GB}$ follow more or less those of $[p_s]_{SH}$ and $[p_w]_{NH}$, respectively, with their maximum (minimum) values occurring in boreal summer (winter). On the other hand, the hemispheric-mean p_d and p_w tendencies of both hemispheres (the top and bottom curves of Fig. 2b) reach their minimum and maximum values, respectively, in spring. Because of these two factors, we present differences of concerned variables between July and January (Fig. 3) to answer the two questions raised in the Introduction: the regional relationship between seasonal variations of p_s and p_w and between atmospheric circulation and water vapor transport. Actually, the differences of p_s and p_w between July and January are approximately equal to twice the amplitudes of their annual cycles.

3.1. Surface pressure

Landmass is warmer than ocean in summer, while this land-ocean thermal contrast is reversed in winter. Airmass, i.e., p_s/g, is heavier (lighter) over landmass and lighter (heavier) over ocean during winter (summer). In other words, the seasonal variation of land-ocean airmass contrast generally follows that of the land-ocean thermal contrast.

(1) Northern hemisphere

In winter, the Aleutian and Icelandic lows deepen, and surface pressure increases over most continents including North America, north Africa and Eurasia. The land-ocean thermal contrast is reversed in summer (compared to winter) and so is the land-ocean contrast of surface pressure. In essence, the development of the North Pacific and North Atlantic anticyclones fills the two oceanic lows. On the other hand, the winter surface highs over continents yield to the summer surface lows to accommodate the major monsoons of Mexico, India and Asia. However, an unusual seasonal variation of p_s exists over the Tibetan Plateau (around 90° E and 30° N); the $\Delta p_s[=p_s\,(\text{July}) - p_s\,(\text{January})]$ anomalies in this region are opposite to the general seasonal p_s variation of winter high -summer low surface pressure over landmass (Saha et al. 1994). For convenience of later discussion, we shall define the difference of any variable's monthly-mean values between July and January as "anomaly". Ignoring the Tibetan Plateau, one can see easily that a distinct and pronounced *east-west* land-ocean contrast prevails the Δp_s anomalies. These Δp_s anomalies may reach as large as 20 mb, but the seasonal variation of $[p_s]_{NH}$ (not shown) is only about 1 mb (smaller than seasonal variation of $[p_s]_{SH}$). The small value of $[p_s]_{NH}$ results primarily from the cancellation of Δp_s anomalies between land and ocean.

(2) Southern hemisphere

Because there is less landmass, the atmospheric flow is much more zonal in the southern hemisphere. The east-west land-ocean contrast of Δp_s anomalies is not as large in the southern hemisphere as in the north. Nevertheless, centers of Δp_s anomalies stand out clearly over all three southern-hemisphere continents. The major seasonal seesaw of Δp_s anomalies is *north-south* between the Antarctic continent and the three southern-hemisphere subtropical continents, rather than the east-west land-ocean contrast seen in the northern hemisphere. $[p_s]_{SH}$ attains its maximum value during southern winter; as inferred from Fig. 3a, this is because the negative Δp_s anomalies around the Antarctic do not offset positive Δp_s anomalies over the three southern-hemisphere continents.

3.2. Water vapor pressure (p_w)

The climatological surface high (low) system is generally associated with low (high) air temperature. Thus, seasonal variation in the land-ocean contrast of p_s is the opposite of that in the land-ocean thermal contrast. According to the Clausius-Clapeyron equation, warmer (colder) air associated with the surface low (high) system may contain more (less) water vapor. Based upon these general relationships between p_s, p_w and air temperature, one may expect that negative Δp_s anomalies are coupled with positive $\Delta p_w\,[=p_w\,(\text{July}) - p_w\,(\text{January})]$ anomalies and vice versa. This argument is confirmed by the contrast between Δp_s and Δp_w anomalies shown in Fig. 3a and b, respectively.

3.3. Local maintenance of Δp_s *and* Δp_w

In principal, seasonal variations of $[p_s]_{GB}$ and $[p_w]_{GB}$ are coincident; this is approximately true to the GEOS-1 data. Some distinctive regional discrepancies between Δp_s and Δp_w should, however, be noticed before we deal with the local maintenance of these two quantities.

(1) Spatial structures of Δp_s and Δp_w anomalies are relatively coherent in the subtropics of both hemispheres with opposite signs, but not in high latitudes. The disappearance of Δp_w in high latitudes is due to the low moisture content.

(2) Δp_s anomalies are generally larger in magnitude than Δp_w anomalies. It is inferred from this contrast in magnitude that the local maintenance mechanisms of these two quantities differ from each other.

In view of their zonally asymmetric components, regional Δp_s and Δp_w anomalies cannot be maintained solely by the Hadley circulation as seen in the hemispheric-mean budgets, but also by the global divergent circulation. According to Boer (1988) and Chen (1985), the global divergent circulation is responsible for the divergent components of airmass and water vapor fluxes, $\langle V_D\rangle\left(=\int_0^{p_s} V\mathrm{d}p = gM_d\right)$ and Q_D. Since $\nabla\cdot\langle V_D\rangle = g\nabla\cdot M_d$ and $\nabla\cdot Q_D = \nabla\cdot Q$, we can use $\langle V_D\rangle$ and Q_D to illustrate the regional maintenance of p_s and p_w, respectively, within the context of eqs. (1) and (2).

The maintenance of Δp_s and Δp_w anomalies

Fig. 3. Differences of various variables $\Delta(\;)$ between July and January: (a) $\Delta[p_s, \langle V_D\rangle]$, (b) $\Delta(p_w, gQ_D)$ and (c) $\Delta[g(E-P), gQ_D]$. Contour intervals of Δp_s, Δp_w and $\Delta[g(E-P)]$ are 4 mb, 0.5 mb and 2 mb, respectively. These variables are stippled in the following way: heavily (lightly) stippled when $\Delta p_s \geqslant 4$ mb ($\leqslant -4$ mb), $\Delta p_w \geqslant 1$ mb ($\leqslant -1$ mb) and $\Delta[g(E-P)] \geqslant 2$ mb ($\leqslant -2$ mb).

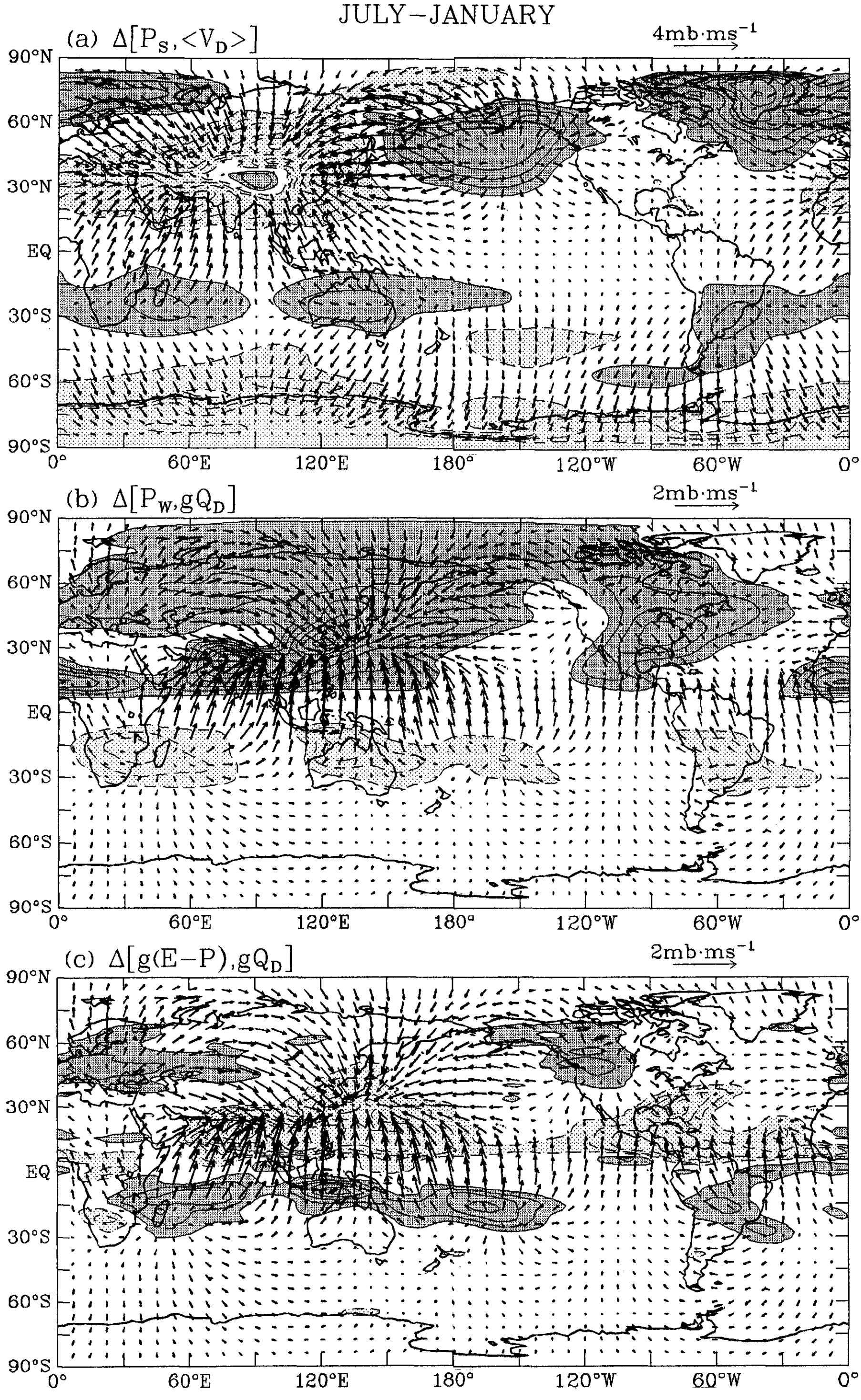
JULY−JANUARY
(a) Δ[P_S,<V_D>]
4mb·ms⁻¹
(b) Δ[P_W,gQ_D]
2mb·ms⁻¹
(c) Δ[g(E−P),gQ_D]
2mb·ms⁻¹
90°N
60°N
30°N
EQ
30°S
60°S
90°S
0°
60°E
120°E
180°
120°W
60°W
0°

may be demonstrated by $\Delta\langle V_D\rangle$ [$=\langle D_D\rangle$ (July) — $\langle V_D\rangle$ (January)] and ΔQ_D [$=Q_D$ (July) — Q_D (January)] vectors superimposed on these anomalies. The salient features of divergent components of airmass and water vapor flux are as follows.

(1) It was pointed out previously that airmass diverges from positive to negative pressure tendency regions. Although Boer (1988) and van den Dool and Saha (1993) computed $\langle V_D\rangle$, the contrast between $\Delta\langle V_D\rangle$ and Δp_s in Fig. 3a shows clearly that airmass diverges from centers of positive to negative Δp_s anomalies. The cross-equator transport of airmass revealed in the hemispheric-mean airmass budget exists mainly between the African continent and the western tropical Pacific.

(2) Without a phase change, water vapor is a passive constituent. Q_D is primarily driven by the lower-tropospheric divergent flow. Recall that centers of positive (negative) Δp_s anomalies coincide with those of negative (positive) Δp_w anomalies. The contrast between Δp_s and ΔQ_D anomalies shows that water vapor converges from centers of negative to positive Δp_w anomalies. The cross-equator transport of water vapor is significant around most parts of the equator. Regionally and hemispherically, water vapor is transported from negative to positive Δp_w regions.

(3) Since water vapor is transported from centers of negative to positive Δp_w anomalies, there must be water vapor source (sink) regions associated with negative (positive) centers of Δp_w anomalies to supply (deplete) the water vapor. Assuming that regional $\partial p_w/\partial t$ is small, the water-vapor budget equation may be approximated as

$$g\nabla\cdot Q\simeq g\,(E-P).$$

We superimpose $\Delta(gQ_D)$ on $\Delta g(E-P)$ in Fig. 3c. Centers of $\Delta g(E-P)$ anomalies exist on each side of the equator and on the equatorward side of Δp_w centers of opposite polarity. The contrast between $\Delta g(E-P)$ and ΔgQ_D reveals that water vapor converges from the water vapor source [$\Delta(E-P)>0$] to the sink [$\Delta(E-P)<0$] region.

As shown by the hemisphere-mean p_w budget, the spring (fall) buildup (decline) of water vapor results from the combining effect of both ΔQ_D and $\Delta(E-P)$. However, from a regional perspective, the water vapor transport by Q_D needs to be supplied by $(E-P)$.

The discussion so far may be summarized as follows.

(1) Patterns of Q_D and $\langle V_D\rangle$ are similar.

(2) Centers of regional Δp_s and Δp_w anomalies are spatially out-of-phase, but the magnitude of Δp_s is much larger than that of Δp_w.

(3) The supply/deplection of water vapor through Q_D is balanced by $(E-P)$.

Regardless of the opposite spatial structure of Δp_s and Δp_w anomalies, $\Delta\langle V_D\rangle$ and ΔQ_D exhibit about the same directions. There must be a link between global divergent circulation and the atmosphere hydrological cycle. It was shown by Chen and Yen (1991) that the global divergent circulation can be maintained in a large part by the tropical diabatic heating:

$$x\simeq\nabla^{-2}\left\{\frac{\partial}{\partial p}\left(\frac{1}{c_p\sigma}\,\dot{Q}\right)\right\}.$$

The diabatic heating is primarily contributed by the release of latent heat by cumulus convection over the water vapor sink [$\Delta(E-P)<0$] region, particularly in the tropics. This heating drives the divergent circulation, which in turn transports airmass in response to the contrast of positive and negative Δp_s anomalies, and transports water vapor to maintain Δp_w anomalies associated with the source and sink regions. The relationship between $\Delta(E-P)$ and $\Delta\langle V_D\rangle$ depicted in Fig. 3 supports the "*water mass forcing*" proposed by van den Dool and Saha (1993) as a mechanism with which atmospheric circulation is driven by water mass sources and sinks.

4. Summary

The findings of this study may be summarized as follows.

(1) Seasonal variations of $\partial[p_w]_{GB}/\partial t$ and $g[E-P]_{GB}$ are comparable in magnitude and approximately synchronous in time with a maximum in boreal spring and a minimum in boreal fall. These seasonal variations manifest a properly balanced global-mean water vapor budget within the GEOS-1 data. The coherent variations of $\partial[p_s]_{GB}/\partial t$ and $\partial[p_w]_{GB}/\partial t$ support previous studies which link the seasonal variation of atmospheric mass to variations in water vapor.

(2) The Hadley circulation is responsible for the equator-crossing airmass and water vapor in the hemispheric-mean budgets of these two quantities, but a quadrature phase relationship exists between

these two physical processes. The hemispheric-mean p_s tendency is maintained solely by the equator-crossing airmass caused by the Hadley circulation. However, the compensation between the water vapor source/sink and the equator-crossing water vapor transport causes the hemispheric-mean p_w tendency to be out-of-phase with the hemispheric mean p_s tendency.

Both p_s and p_w departures from their annual-mean values exhibit a pronounced signature of land-ocean contrast, but a spatially out-of-phase relationship exists between centers of p_s and p_w departures. The p_s departures are maintained by the global divergent circulation in such a way that airmass diverges from centers of positive to negative p_s departures. In contrast, water vapor converges by the global divergent circulation from centers of negative to positive p_w departures. Since the water vapor sinks and sources are generally associated with centers of positive and negative p_w departures, respectively, the global divergent circulation, which transports airmass and water vapor, is driven by diabatic heating which draws its major contribution from the latent heat released by cumulus convection. The link between the global divergent circulation and the water vapor source/sink matches well with the water mass forcing proposed by van den Dool and Saha (1993).

5. Acknowledgements

This study is supported by the NSF Grant ATM-9416954 and the NASA Grant NAG5–2930. The comments offered by Dr. H. van den Dool are helpful in clarifying some issues discussed in this paper. We would like to thank Mrs. Reatha Deidrichs for her typing support and Mrs. Susan Carr for her editing assistance.

REFERENCES

Bloom, S. C., L. L. Tackacs, A. M. da Silva and D. Ledvina, 1996. Data assimilation using incremental analysis updates. *Mon. Wea. Rev.* **124**, 1256–1271.

Chen, T.-C. 1985. Global water vapor flux and maintenance during FGGE. *Mon. Wea. Rev.* **113**, 1801–1819.

Chen, T.-C. and M.-C. Yen, 1991. Interaction between intraseasonal oscillations of the midlatitude flow and tropical convection during 1979 northern summer: The Pacific Ocean. *J. Climate* **4**, 653–671.

Chen, T.-C. and Pfaendtner, 1995. Low-frequency variations in the atmospheric branch of the global hydrological cycle. *J. Climate* **8**, 92–107.

Chen, T.-C., M.-C. Yen, J. Pfaendtner and Y. C. Sud, 1996. Annual variation of the global precipitable water and Its maintenance; Observation and climate-simulation. *Tellus* **49A**, 1–16.

Saha, K., H. van den Dool and S. Saha, 1994. On the annual cycle in surface pressure on the Tibetan Plateau compared to its surroundings. *J. Climate* **7**, 2014–2019.

Schubert, S. D., R. B. Rood and J. Pfaendtner, 1993. An assimilated data set for earth science application. *Bull. Amer. Meteor. Soc.* **74**, 2331–2342.

Schubert, S. D., C.-K. Park, C.-Y. Wu, W. Higgins, Y. Kondratyeoa, A. Malod, L. Takacs, M. Seablom, and R. Rood, 1995. *A multiyear assimilation with the GEOS-1 system: Overview and result.* NASA tech. Memo. 104606, Vol. 6, 183 pp. (Available from the NASA Center for Aerospace Information, 800 Elkridge Landing Rd., Linthicum Heights).

Trenberth, K. E., J. R. Christy and J. G. Olson, 1987. Global atmospheric mass, surface pressure, and water vapor variations. *J. Geophys. Res.* **92**, 815–814, 826.

Van den Dool, H. and S. Saha, 1993. Seasonal redistribution and conservation of atmospheric mass in a general circulation model. *J. Climate* **6**, 22–30.

Van den Dool, H., J. Schemn and S. Saha, 1995. On the climatological annual cycle in global mean atmosphric surface pressure and hydrology as revealed by NCEP/NCAR reanalysis. *Proceedings of the 20th Climate Diagnostic Workshiop*, Seattle, Washington, Oct. 23–27, 1995, p. 366–369.